Large strain viscoelastic dissipation during interfacial rupture in laminated glass

Paul Elzière, Cécile Dalle-Ferrier, Etienne Barthel, Costantino Creton, Matteo Ciccotti

Large strain viscoelastic dissipation during interfacial rupture in laminated glass

Paul Elzière[a,b], Cécile Dalle-Ferrier[b], Costantino Creton[a], Étienne Barthel[a] and Matteo Ciccotti[a]

In the dynamic rupture of laminated glass, it is essential to maximize energy dissipation. To investigate the mechanisms of energy dissipation we have experimentally studied the delamination and stretching of a polymeric viscoelastic interlayer sandwiched between glass plates. We find that there is a velocity and temperature domain in which delamination fronts propagate in a steady state manner. At lower velocities, fronts are unstable while at higher velocities, the polymer ruptures. Studying the influence of the interlayer thickness, we have shown that the macroscopic work of fracture during the delamination of the interlayer can be divided in two main components: 1. A near crack work of fracture which is related to the interfacial rupture and to the polymer deformation in the crack vicinity. 2. A bulk stretching work which relates to the stretching of the interlayer behind the delamination front. Digital Image Correlation measurements showed that the characteristic length scale over which this stretching occurs is of the order of the interlayer thickness. Finally, an estimate of the bulk stretching work was provided, based on a simple uniaxial tensile test.

1 Introduction

A very useful and interesting material that is ubiquitous in our daily lives is laminated glass, a layered composite where a polymer layer is sandwiched between two glass plates in order to provide impact resistance to transparent glass panels such as car windshields or glass floors. When laminated glass is impacted by a hard object at high enough speed, multiple cracks propagate in the glass layers with little energy dissipation and the expected fracture resistance arises from the presence of a viscoelastic polymer interlayer which dissipates most of the energy of the impact, as it delaminates from the glass and is stretched extensively.

Several studies have tried to model the impact process in its full complexity. They considered various loading conditions in finite element analysis: blast resistance[1], ball drop tests[2] or headform impact[3]. At this level of macroscopic description, the complexity of the impact problem and the complex rheological properties of the polymer preclude a precise description of the dissipation mechanisms.

Model experimental setups have been developed to improve the understanding of the different energy dissipation mechanisms involved during the impact. During impact the broken glass pieces undergo a membrane stretch and the glass shards move away from each other. This leads to the delamination of the interlayer and its subsequent stretching. We mainly focused on a Through Crack Tensile test (TCT Test, Figure 1). This test reproduces the uniaxial stretching of the delaminated interlayer and has been used in several previous studies on laminated glass[4–6]. These studies have emphasized the importance of the deformation of the viscoelastic interlayer in the dissipative processes.

An interesting result stemming from the TCT Test is the existence of a steady state delamination regime. *Sha et al.*[4] observed a constant level of force and strain during the delamination and were able to perform an estimate of the adhesion energy with finite element calculations. *Sha et al.* described the interlayer as a linear viscoelastic material and the interface was modeled with cohesive elements. The order of magnitude of the glass/interlayer fracture toughness was found close to 100 $J.m^{-2}$ (at room temperature and for a controlled displacement speed of ≈ 0.01 $mm.s^{-1}$). *Muralidhar et al.*[5] added to the previous description by using a visco-hyperelastic model for the interlayer. This model gave a better qualitative description of the experiments. Moreover, they pointed out that the large observed macroscopic work of fracture comes from both the deformation of the bulk material and the interfacial fracture processes. A similar separation of the macroscopic work of fracture into bulk and interfacial contributions has been previously described also by *Rahulkumar et al.*[7]. The coexistence of different dissipation regimes, length scales and zones was also used in several attempts to explain the large amount of dissipated energy measured during the tearing of viscoelastic materials or during the debonding of a viscoelastic polymer from a rigid surface[8–11]. Only a few experimental studies have focused on the details of the de-

[a] *Laboratoire Sciences et Ingénierie de la Matière Molle, PSL Research University, UPMC Univ Paris 06, ESPCI Paris, CNRS, 10 rue Vauquelin, 75231 Paris cedex 05, France*
E-mail: etienne.barthel@espci.fr; matteo.ciccotti@espci.fr
[b] *Saint-Gobain, 39 quai Lucien Lefranc, 93300 Aubervilliers, France.*

formation field near the crack tip for such materials [12].

In this paper, we will show that in the TCT Test, a steady state delamination regime can only be achieved for certain conditions of applied velocity and temperature. In this steady state regime, the macroscopic work of fracture will be estimated and separated in two components: a bulk stretching work and a near crack work of fracture. We will show that most of the energy is dissipated by the stretching of the material over a length close to the interlayer thickness. In this stretching zone, we will finally explain the large macroscopic work of fracture by both the high strain level and the important strain rate.

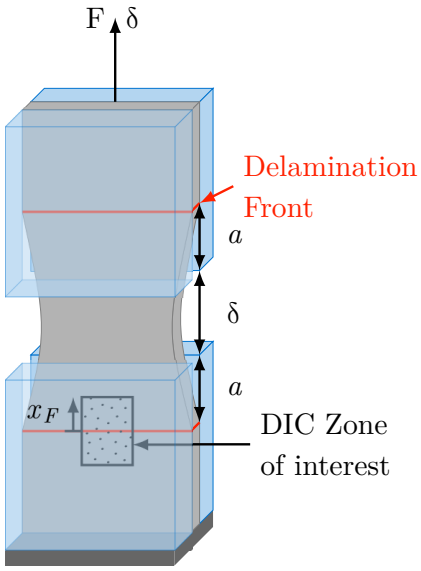

Fig. 1 Through Crack Tensile Test (TCT Test) model experiment. A uniaxial tensile test is conducted on a pre-cracked laminated glass sample. The interlayer is stretched in-between the delamination fronts which propagate in opposite directions.

2 Methods

2.1 Interlayer

The interlayer is a standard industrial Poly(vinylbutyral) with a glass transition around 20 °C. More details on the material can be found in *Elziere* [13].

2.2 Uniaxial tensile test

Uniaxial tensile tests were carried out to characterize the large strain behavior of the interlayer. The tensile experiments were conducted on bone shaped samples that had 0.76 mm thickness, 4 mm width and an active length of 20 mm.

For higher forces (at higher strain rates and lower temperatures), the tests were carried out on a Zwick/Roell Hamsler HC25 hydraulic machine with a load cell of 1kN. For lower forces (at lower strain rates and higher temperatures), the tests were conducted on a Instron 5565 machine with 10 N and 100 N load cells.

Temperature was controlled by a PID thermoregulator 2216L from Eurotherm Automation in a temperature chamber.

2.3 Preparation of laminated glass

Model laminated glasses were assembled in a clean room. The 2 mm-thick glasses were cleaned with a standard industrial soap solution and dried with air. The glasses were then assembled with the interlayer. The samples were heated at high temperature in an autoclave for 1.5 hours at 140 °C and 10 bar, resulting in very good adhesion at the two glass/polymer interfaces.

The TCT Test samples were prepared with an interlayer thickness ranging from 0.38 to 1.52 mm. The reference interlayer was 0.76 mm in thickness. The samples were 50 mm in width and 100 mm in length.

2.4 Through Crack Tensile Test (TCT Test)

Model laminated glass samples were tested in a custom experiment to study the delamination of the interlayer from the glass. For the TCT Test, the two glass plates were pre-cracked. Cracks were propagated on each glass side in the middle of the plate.

The through crack tensile tests (Figure 1) were conducted on the Zwick/Roell machine with a 10 kN load cell. The tests were conducted at fixed grip velocity ranging from 0.01 to 100 mm.s^{-1}.

Displacements were measured with a Baumer VLG-20M video camera. Frames were acquired with a Matlab®(R2015a) Video Acquisition toolbox.

2.5 Digital image correlation DIC

Some TCT Test samples were modified to measure the local displacement field in the interlayer during delamination by digital image correlation. Paint was randomly spread to form a speckle of points (approximately 10 μm size) on one side of an interlayer piece with half the standard thickness. Another half thickness interlayer was juxtaposed to this one and the laminated structure was assembled as sketched in Figure 2. As a result the paint dots were placed on the midplane of the structure.

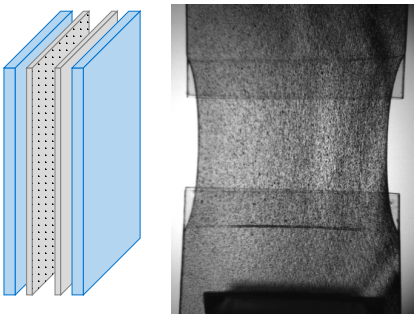

Fig. 2 Experimental setup of the digital image correlation. Paint was randomly spread on one face of an interlayer sheet to form a speckle. The sample width is 50 mm.

Frames were captured with a Photron Mini UX100 fast camera at 125 fps with a Questar QM1 long distance microscope (resolution of 3 μm/px). Image treatment was done in Matlab®R2015a with the CORRELI Q4 digital image correlation program [14]. The mesh size of the finite element grid used by the software was set to 30 μm. A regularization length of 0.6 mm was used during all calculations.

3 Results

3.1 Large strain behavior of the interlayer in uniaxial tension

During the impact or during the TCT Test, the delaminated interlayer is stretched up to large deformations leading to a high amount of dissipated energy[15]. To fully characterize this dissipation process, the mechanical response of the interlayer itself was characterized in the large strain regime and at various strain rates. Uniaxial tensile tests up to a stretch of 3 were performed on the interlayer. These experiments were conducted at 20 °C for four different stretch rates: 0.001, 0.01, 0.1 and 1 s^{-1}. Two additional tests were conducted at 10 and 50 °C at 1 s^{-1}. The crosshead velocity was constant during the loading and the unloading and thus the instantaneous strain rate decreases as the stretch increases.

Figure 3 shows the true stress σ_T against stretch λ_T of the interlayer in a cyclic uniaxial tensile test. The test carried out at 10 °C is representative of the behavior in the glassy regime, while the test at 50 °C is representative of the rubbery regime. The results at 20 °C are close to the glass transition of the interlayer, which spans from 20 °C to 30 °C.

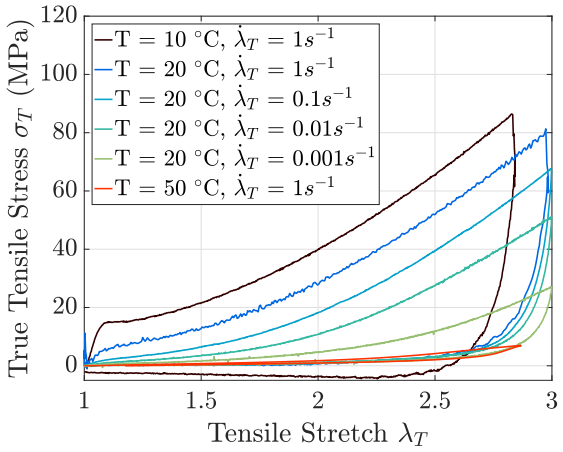

Fig. 3 Uniaxial cyclic tensile tests at 10, 20 and 50 °C on the interlayer up to a stretch of 3 at different stretch rates.

The complex large strain behavior of the interlayer involves a non-linear response, an important dissipation and a time dependent behavior. At low temperature, the material creeps back to its original shape within a few minutes after unloading. The initial modulus at 1 s^{-1} varies from 1 MPa at 50 °C to 200 MPa at 10 °C. At 20 °C and low strain rates (0.001 s^{-1}) or at 50 °C, the interlayer behaves as a viscoelastic rubber. At higher stretch rates such as 1 s^{-1} at 20 °C and at 10 °C, the interlayer displays an elastic-plastic like behavior, with a yield stress followed by a plateau for stretches varying from 1.1 to 1.4. During the unloading part, the stress relaxes rapidly and at about a stretch of 2, the sample buckles and the curve is not representative anymore of the real behavior. However, after the cyclic experiment at 10 °C and 20 °C, the sample recovers its initial shape in 1 to 2 min at room temperature. This behavior is not observed at 50 °C where a permanent stretch of about 1.1 is observed.

The volume density of dissipated energy in a cycle $\mathscr{E}_{diss}$ is defined as the difference between the area under the loading and unloading curves (Insert Figure 4). The ratio of dissipated energy over the total work of external forces $\mathscr{W}_{ext}$ is denoted $R_d = \mathscr{E}_{diss}/\mathscr{W}_{ext}$ and is plotted as a function of time and temperature in Figure 4. R_d ranges from 75 to 85% at 20 °C, it is above 95% at 10 °C and it is close to 40% at 50 °C.

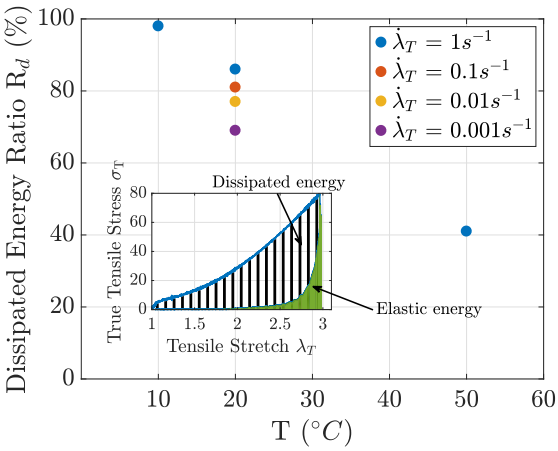

Fig. 4 Dissipated energy ratio, namely dissipated energy over total work of external forces, as a function of time and temperature. In the insert, the highlighted areas correspond to dissipated energy (dark hashed) and elastically stored energy (plain green) on a uniaxial tensile test response at 20 °C and 1 s^{-1}

.

3.2 Steady state in a Through Crack Tensile Test

A typical TCT Test is shown in Figure 5 for a temperature of 20 °C, a constant velocity $\dot{\delta} = 10$ mm.s^{-1} applied to the upper clamped glass and an interlayer thickness $h = 0.76$ mm. These test conditions will be used as the reference conditions in this study. In this experiment, four delamination fronts (two on each glass pane – front and back – on the top glass and on the bottom glass) propagate at a constant velocity in opposite directions. We denote a the delaminated length on each side, which is measured as the distance between the edge of the glass plate and the delamination front (Figure 5). In between these fronts the delaminated interlayer of initial length $2a$ is stretched to the length $\delta + 2a$. The mean stretch of the delaminated interlayer $\bar{\lambda}_{\text{TCTT}}$ is thus given by:

$$\bar{\lambda}_{\text{TCTT}} = \frac{\delta + 2a}{2a} \tag{1}$$

As found in previous studies[5,6], a steady state regime with constant force is observed during the delamination. As shown in Figure 6, the delamination force F_{TCTT} first goes through a peak and then stabilizes to a steady state value F^0_{TCTT} when the delaminated length a becomes larger than the interlayer thickness h. The mean stretch also rapidly reaches a plateau value $\bar{\lambda}^0_{\text{TCTT}}$ in time (Figure 6). This result can be retrieved by plotting, as in the insert, the length of the stretched delaminated interlayer $\delta + 2a$ as a function of its intial length $2a$. The fronts propagate symmetrically and the slope of this curve gives $\bar{\lambda}^0_{\text{TCTT}}$ about 2.4 in this case.

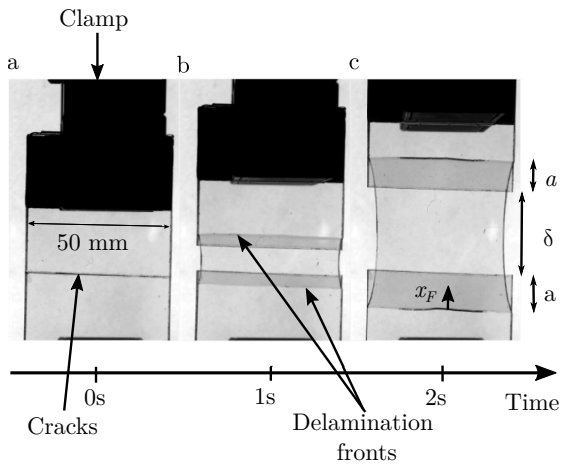

Fig. 5 A typical TCT Test at 20 °C and 10 mm.s^{-1} versus time. The sample width is 50 mm. The displacement of the upper clamped glass is called δ. The crack front position relative to the glass edge is noted a. The position of a given point in the reference frame of the lower delamination front is x_F.

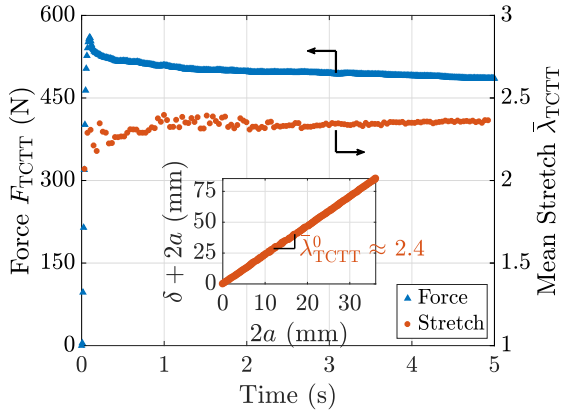

Fig. 6 Delamination force and mean stretch rapidly reach a steady state during a TCT Test at 20 °C and 10 mm.s^{-1}. In the insert, the mean stretch $\bar{\lambda}_{\mathrm{TCTT}}$ is defined as the ratio of the length of the stretched delaminated interlayer $\delta + 2a$ over its initial length $2a$.

3.3 Effect of velocity and temperature: delamination phase diagram

Beyond the reference test conditions, the time and temperature dependence of the TCT Test response were also explored. TCT Tests were performed at three different temperatures (5, 20 and 50 °C) and different crosshead velocities ranging from 1 to 60 mm.s^{-1}.

The steady state delamination process described in the previous part is not observed for all temperatures and velocities. At lower imposed velocities, the delamination front is unstable and starts to undulate. Propagation often stops after some time leading to a sudden increase of the mean stretch and eventually to the rupture of the interlayer through the propagation of a blunted crack. At higher imposed velocities, even if the delamination initially proceeds in a steady state regime, the delamination is prematurely interrupted by the sudden rupture of the interlayer through the propagation of a sharp brittle crack. In the present work, we will only focus on the measurements in the steady state regime where delamination is stable.

In Figure 7, the delamination force in the steady state regime F^0_{TCTT} is plotted as a function of tensile velocity $\dot{\delta}$ for various temperatures. The delamination force increases as the velocity increases or the temperature decreases. The limits between the three regimes are also roughly estimated and drawn on the graph (dark lines). We remark that only the data points in the intermediate regime can be reported since the steady state force is not defined for the unstable regimes.

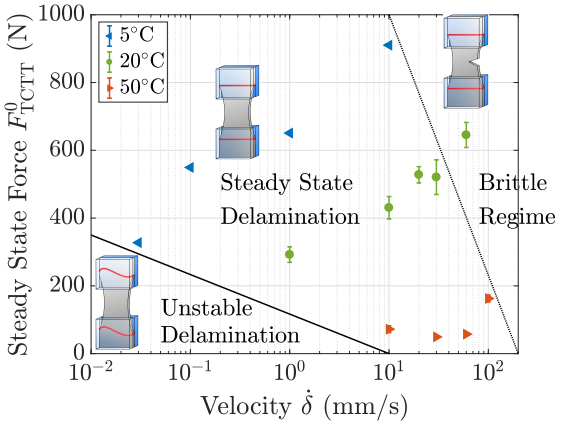

Fig. 7 The steady state delamination force F^0_{TCTT} increases with speed and decreases with temperature. The dark lines roughly delimit the three delamination regimes. Data points can only be reported in the intermediate regime where no undulation of the front (low speed and high temperature) or brittle behavior (high speed and low temperature) were observed.

In Figure 8, the mean stretch in steady state $\bar{\lambda}^0_{\mathrm{TCTT}}$ is plotted as a function of applied velocity $\dot{\delta}$ and temperature. The measurements cover the stable delamination regime at each temperature. At 5 °C, the stretch ranges from 2.05 to 2.3, at 20 °C it ranges from 2.1 to 2.6 and at 50 °C it ranges from 2.8 to 3.05 for the different speeds. While the stretch is more or less constant within the error bars at both 5 °C and 50 °C, it displays a significant increase with velocity at 20 °C.

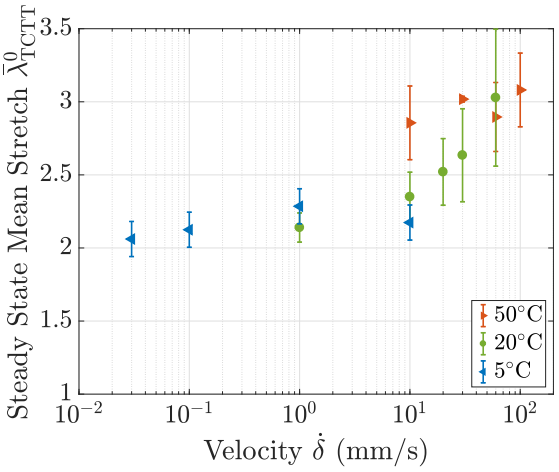

Fig. 8 Dependence of the mean stretch in the steady state regime with velocity and temperature.

3.4 Measurement of the strain field by DIC

The strain field in the delaminated interlayer appears to be quite homogeneous in space except in the neighborhood of the delamination fronts. This can first be inferred from Figure 5(c), showing that the width of the interlayer becomes constant at a certain distance from the delamination front. In order to obtain a better description of the stretch field, digital image correlation experiments were performed during the delamination of patterned TCT Test samples (as described in section 2.5).

To determine the length scale of the stretch gradient, TCT Test were performed in the reference steady state condition (10 mm.s^{-1} and 20 °C) for two different values of interlayer thickness: 0.76 and 1.52 mm. The speed of the delamination fronts was found to be almost identical for both thicknesses (respectively 3 and 4 mm.s^{-1}). The mean stretch $\bar{\lambda}^0_{TCTT}$ reached during the steady state delamination far from the fronts is close to its mean value $\bar{\lambda}^0_{TCTT}$, which was found to be equal to 2.3 and 2.1 respectively.

The displacement field is measured along a vertical line parallel to the traction axis (white line in in Figure 9). From this displacement field, the interlayer stretch field $\lambda_{DIC}(x_f)$ is determined as a function of the distance x_f from the lower delamination front. The results are represented in Figure 10 after normalizing the nominal strain field $\varepsilon^N_{DIC} = \lambda_{DIC} - 1$ to its mean value $\bar{\varepsilon}^{N0}_{TCTT} = \bar{\lambda}^0_{TCTT} - 1$. The distance to the delamination front x_F is normalized by the interlayer thickness h.

In the region A of the curve in Figure 10, the interlayer deforms up to a fraction of about 60% of $\bar{\varepsilon}^{N0}_{TCTT}$ on a length close to the interlayer thickness h. The corresponding value of the stretch will be denoted $\bar{\lambda}^*_{TCTT}$. After this sharp increase of the strain, the polymer reaches the steady state maximal stretch (which is found to be close to the mean value $\bar{\varepsilon}^{N0}_{TCTT}$) over a much longer distance of the order of the sample width w (region B).

As this stretching occurs in a steady state regime, the stretch rate can be calculated using the delamination front speed. At 20 °C and for an applied velocity of 10 mm.s^{-1}, the stretch rate in region A is about 3 s^{-1} for the 0.76 mm thickness interlayer and about 1.5 s^{-1} for the 1.52 mm thickness interlayer. The stretch rate in region B is lower (about 0.5 s^{-1}) and is essentially independent of the sample thickness. Finally, in the middle region of the interlayer, at a distance larger than w from the delamination front, the stretch is essentially constant during delamination and the stretch rate in this region is vanishing.

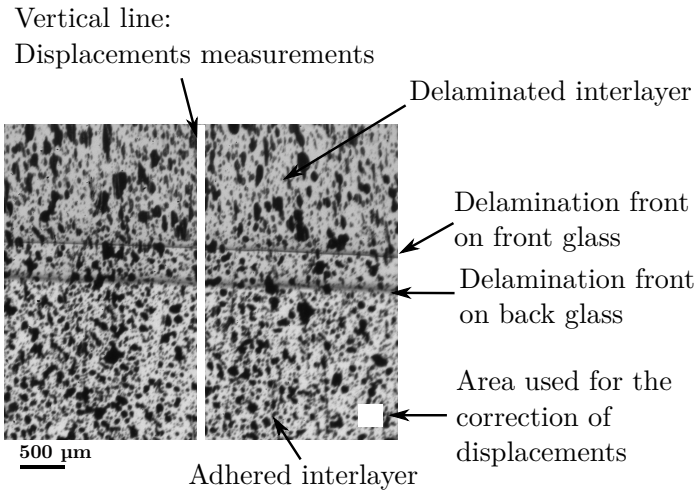

Fig. 9 Digital image correlation frame. The displacements measured on the vertical white line are corrected by the displacements (supposed to be due to experimental noise) of the white square region out of the delaminated area.

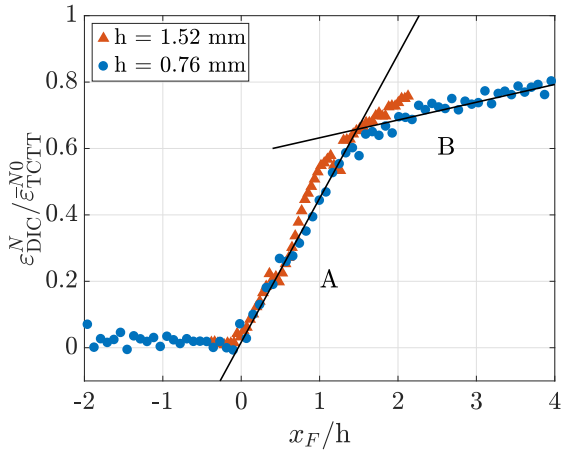

Fig. 10 Local stretch measurements through digital image correlation at 20 °C and 10 mm.s^{-1}. Two thicknesses h were tested. Two stretch rate regions are identified ahead of the crack front. The first region A spans on a length close to the interlayer thickness h. The second region B spans on a length close to the specimen width w.

3.5 Influence of the interlayer thickness

As observed in the previous section, most of the stretching of the interlayer during steady state delamination is rapidly reached over a length scale roughly equal to the interlayer thickness h and with a local stretch rate that is roughly inversely proportional to h. Hence, the interlayer thickness should have a major influence on the overall TCT Test response. A TCT Test was thus conducted with four different interlayer thicknesses: 0.38, 0.76, 1.14 and 1.52 mm in

the steady state delamination regime at the reference conditions: 20 °C and 10 mm.s^{-1}. As reported in Figure 11 the increase in the interlayer thickness leads to a proportional increase in the measured steady state force F^0_{TCTT} from 220 to 710 N, while the interlayer mean stretch ($\bar{\lambda}^0_{\mathrm{TCTT}}$) decreases slightly from 2.4 to 2.2.

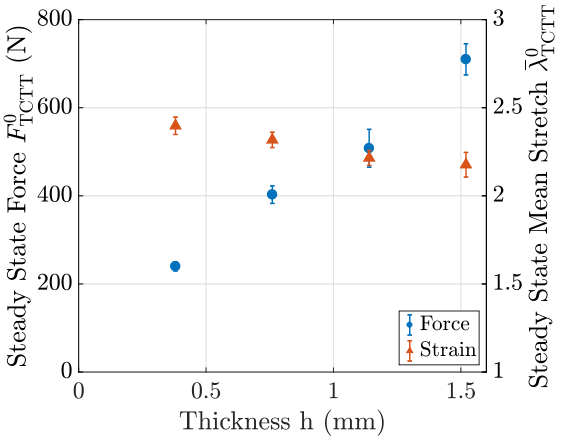

Fig. 11 Force (blue circles) and mean stretch (red triangles) measured for different interlayer thicknesses during a TCT Test at 20 °C and 10 mm.s^{-1}.

4 Discussion and modeling

During the reference TCT Test at 20 °C and 10 mm.s^{-1}, the interlayer is stretched from $\lambda = 1$ to about 2.4 and most of this stretching occurs over a length equal to the interlayer thickness h, which induces high local strain rates (of the order of 3 s^{-1} for the standard thickness of 0.76 mm). The large strain properties of the interlayer (reported in section 3.1) suggest that in this range of temperature and stretch rate most of the external work provided to stretch the interlayer is dissipated. During the delamination of the interlayer, the stretching of this local region of size h might thus induce a large amount of dissipated energy to be added to the energy cost for propagating the interface cracks.

In the literature, the elevated level of dissipation during the tearing of a viscoelastic material or during the separation between a viscoelastic polymer and a rigid elastic substrate has long been a puzzling problem[11,16,17]. During the fracture of a viscoelastic material, even if the rupture of the chemical or physical bonds only requires 0.1 to 10 J.m^{-2}, large macroscopic works of fracture of the order of 1 kJ.m^{-2} are generally recorded. Most approaches developed between the '70s and '80s are based on perturbations of the crack tip stress field of linear elastic fracture mechanics. These perturbations involve the local energy dissipation due to viscoelastic or plastic constitutive laws of the materaial, while preserving linear elastic behavior in the far field.

Schapery[8] and *De Gennes*[9] suggested that because of the time dependency of the polymer behavior, there were several separate dissipation zones ahead of the crack tip. Later *Saulnier et al.*[18] and *Persson et al.*[19] have shown that this simple linear viscoelastic description of the material can support a large dissipated energy amplification observed during the crack propagation. However, *Gent*[10] has shown that when combining the time-temperature equivalence determined from the linear rheology of the viscoelastic material with the velocity-temperature dependence of the measured work of fracture, this leads to estimating an unrealistically small size for the dissipation zone at the crack tip, close to 1 Å. *Barthel and Fretigny*[20] have derived an improved formulation for a fully linear viscoelastic system that highlights the importance of the coupling between the remote loading and the crack tip dissipation phenomenon through an intermediate viscoelastic dissipation zone. *Hui et al.*[21] have shown that for soft elastic materials the crack tip region is elastically blunted by local large strains over a region of typical size Γ_{crack}/E that can be millimetric in size for rubber-like materials. As explained by *Creton and Ciccotti*[11,22] this implies that for soft viscoelastic materials the large strain region and the dissipative regions are generally strongly coupled and the large strain behaviour is the relevant one for modeling the dissipation associated to crack propagation. Moreover, when the thickness of confined soft materials becomes comparable to the large strain dissipative region, the large strain dissipation in the bulk of the sample can also become a significant contribution to the total work of fracture and the issue of separability of the interfacial terms is presently an important open issue.

In the present section the delamination results will be used to determine the macroscopic work of fracture needed to delaminate the soft viscoelastic confined layer in the steady state regime. Then, different dissipation zones will be identified and the dissipation processes will be connected to the intrinsic mechanical behavior of the interlayer. Finally, the emerging model will be used to explain some of the previous experimental observations.

4.1 Macroscopic work of fracture

Since the interlayer is stretched during delamination, the macroscopic work of fracture is either stored elastically or dissipated due to the viscous and plastic components of the interlayer rheology. Only a small amount of the input energy will reach the delamination front and will serve to break the interfacial bonds between the interlayer and the glass.

Using the previous measurements, the overall macroscopic work of fracture G_m for steady state delamination can be evaluated as follows:

$$G_m = \frac{\partial W}{\partial A} = \frac{F^0_{\mathrm{TCTT}}}{w}.(\bar{\lambda}^0_{\mathrm{TCTT}} - 1) \qquad (2)$$

where w is the width of the sample ($w = 50$ mm). At 20 °C and 10 mm.s^{-1}, G_m is about 11 kJ.m^{-2} for the standard thickness ($h =$ 0.76 mm).

The definition of G_m does not correspond to the classical strain energy release rate, since it only contains the dominant term constituted by the work of external forces per unit delaminated area. This quantity is experimentally very well defined, since it corresponds to the measured macroscopic work injected in the system to delaminate the sample. When dealing with soft viscoelastic confined materials, it would be very difficult to properly account for the variations of the stored elastic energy during crack propagation. The strain energy release rate is thus an ill defined quantity that should be treated with caution. On the other hand, since the PVB interlayer proved to be a very dissipative material in the do-

main of stretch rate and temperature used here, the stored elastic energy is a small fraction of the total work for stretching the interlayer (c.f. section 3.1). The macroscopic work of fracture can thus be considered to be close to the strain energy release rate under these circumstances.

4.2 Identification of the different dissipation zones

During a zero angle peel test of a thin layer made of a purely elastic material from a rigid substrate, a significant portion* of the macroscopic work of fracture is stored elastically in the stretched delaminated polymer, while the remaining part is consumed in complex crack tip processes. Under these circumstances the strain energy release rate can be evaluated properly and it provides a direct access to the energy dissipated in the crack tip region.

Collino et al.[23] and *Ponce et al.*[24] have shown that when frictional sliding is allowed during the peeling of an elastomeric material from a rigid substrate at low peel angle, a steady state delamination can occur and far from the delamination front the polymer reaches a homogeneous strain in a similar configuration to the TCT Test. Dissipation was shown to occur in two different zones: a first dissipation zone is associated with the propagation of the crack front, while a second larger region is due to the interface slip over a long distance ahead of the front and contributes the dominant term of the total dissipated energy. Although the delaminated interlayer is stretched over a length equal to the sample width, little energy is dissipated in this region by bulk viscoelasticity due to the weak dissipation presented by these elastomers. The large viscous and plastic dissipation of the laminated glass interlayer presented here complicates this description by adding a dissipation region in the stretched interlayer.

Amouroux et al.[25] and *Newby and Chaudhury*[26,27] have also shown that during the peeling of a viscoelastic adhesive tape on a sliding substrate, energy is dissipated in different zones: interface sliding, near crack viscoelastic losses and bulk viscoelastic dissipation due to the polymer deformation in the bulk of the film, although the large stretch of the peeled tape is prevented by the presence of a stiff backing.

During the steady state delamination of the interlayer in a TCT Test, several of these dissipation regions are combined and potentially strongly coupled. Similarly to the Essential Work of Fracture approach, commonly used for fracture of ductile semi-crystalline materials[28–30], we can tentatively separate the bulk stretching work Γ_{bulk} due to the deformation of the interlayer from a near crack work of fracture Γ_{crack}, which includes the interfacial bond rupture between the interlayer and the glass as well as the near crack deformation of the polymer.

In order to separate these two different dissipative contributions, the variation of the macroscopic work of fracture with the interlayer thickness can be extracted from previous results in standard conditions. G_m is found to increase affinely with the interlayer thickness from 4 to 16 kJ.m^{-2}. The slope of this curve is about 8 MJ.m^{-3}. The extrapolation of this line to a zero thickness interlayer gives a non null intercept at 4 kJ.m^{-2}.

∗ This portion is half if the material peels in its linear elastic regime.

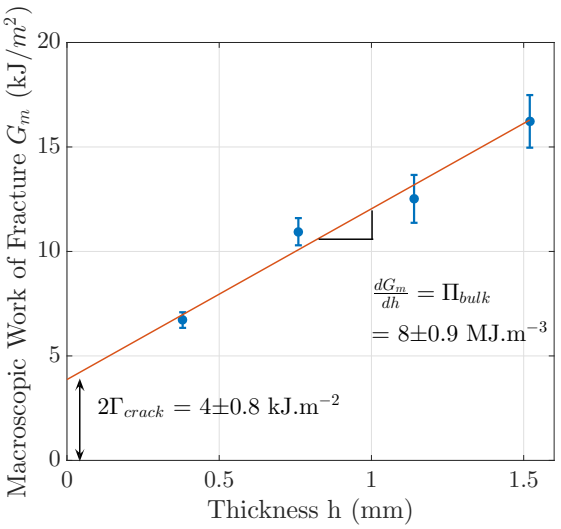

Fig. 12 Macroscopic work of fracture required to delaminate different laminated glass samples with increasing interlayer thicknesses at 10 mm.s^{-1} and 20 °C

The near crack processes will depend on the mode mixity of the loading and on the interlayer confinement, but in the explored range of interlayer thicknesses these do not depend on the thickness. Hence, on Figure 12 the slope of the line gives the volume density (Π_{bulk}) of the bulk stretching work: $\Gamma_{bulk} = \Pi_{bulk} h$. In the full sample there are four similar regions close to the delamination fronts in which the near crack work of fracture Γ_{crack} (per unit area) is dissipated. Since cracks propagate symmetrically, half the sample is considered here and the intercept of the previous line gives $2\Gamma_{crack}$. Thus, the macroscopic work of fracture is:

$$G_m = 2\Gamma_{crack} + \Pi_{bulk} h \tag{3}$$

Γ_{crack} represents the energy dissipated near one single crack front. Π_{bulk} is the energy volume density stored and dissipated by stretching the bulk of the interlayer from 0% to $\bar{\varepsilon}^0_{\text{TCTT}}$.

In the steady state delamination regime the stretching of the interlayer can be schematically separated into four zones as depicted in Figure 13. The following picture arises:

- Zone 1: The near crack tip work of fracture Γ_{crack} is dissipated in the vicinity of each delamination front, where strain rate fields are dominated by the advancing stress concentration region.
- Zone 2: In this fast stretching zone, the interlayer is rapidly stretched from 1 to $\bar{\lambda}^*_{\text{TCTT}}$, which represents 60% of the steady state mean value $\bar{\lambda}^0_{\text{TCTT}}$. This stretching occurs over a length that is comparable to the interlayer thickness h. It is in this fast stretching zone that most of the bulk stretching work $\Gamma_{bulk} = \Pi_{bulk} h$ is dissipated. Π_{bulk} is the volume density of this work.
- Zone 3: In this intermediate zone, the polymer is stretched from $\bar{\lambda}^*_{\text{TCTT}}$ up to the maximal stretch $\bar{\lambda}^0_{\text{TCTT}}$ far from the delamination front over a longer region (length equivalent to the sample width w) and at a much slower pace.

- Zone 4: The middle region of the sample is essentially inactive since the stretch is constant both in time and space, and stress relaxation is negligible during the time scale of the experiment. On the other hand, if we only consider one half of the sample, as in Figure 13, the large macroscopic work of fracture G_m is provided at the free end of this region.

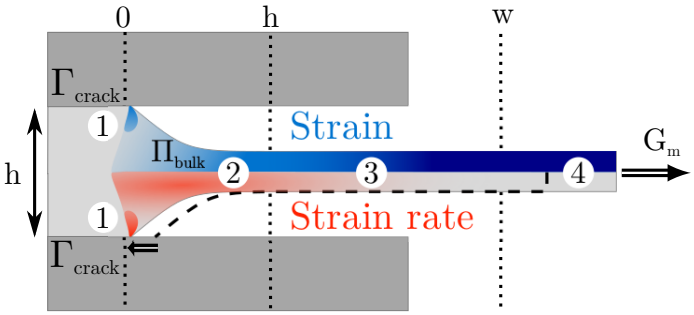

Fig. 13 Far field/crack tip link and energy dissipation during steady state delamination. The stretching of the interlayer can be schematically separated into four zones described in the text. The blue shading in the upper part of the interlayer represents the intensity of the local strain. The reds shading in the lower part represents the local strain rate and is linked to energy dissipation. The dashed line represents the interlayer profile at a previous time during delamination.

4.3 Modeling the bulk dissipation

The leading term in the dissipation during steady state delamination is given by the fast stretching zone, where the interlayer undergoes the largest portion of its stretch and at the highest stretch rate. Although the interlayer undergoes a progressive loss of constraint when stepping though the zones 2, 3 and 4 (c.f. Fig. 13), a uniaxial tensile test at the appropriate stretch rate can provide a good approximation for the amount of dissipated energy in these zones. We remark that the stretching of the interlayer ligament is similar to the stretching of fibrils during the peeling of pressure sensitive adhesives from a rigid substrate[22] or from a tack test and the analogy between fibril stretching and homogeneous uniaxial tension tests has been done previously for soft solids[31] and for liquids[32]. Another analogous fibril stretching phenomenon occurs at a completely different length scale in the widening of crazes in glassy polymers[33]. In all these cases the polymer is stretched up to very large strains at relatively high strain rates leading to large amount of dissipated energy. However, the level of localization of the "active" high strain rate region will depend on the details of the non-linear behavior. In the case of the extension of craze fibrils in a polymer glass the extension from $\lambda = 1$ to $\lambda = 4$ occurs over the first few nm of a μm long fibril[34]. The relevant stretch rate should thus be estimated at this local scale and is much larger than the average strain rate in a very similar way to the case of the TCT Test.

In order to understand why the bulk component of G_m is proportional to the interlayer thickness, the volume of polymer involved in the stretching as the front advances by a distance da has to be evaluated. As a remote loading displacement dδ is applied with a constant loading speed $\dot{\delta}$ that corresponds to a constant measured force F_{TCTT}, the four crack fronts will simultaneously move a distance da. As described before, the delamination fronts are moving at a constant speed and the following relationship can be written:

$$\mathrm{d}a = \dot{a}\mathrm{d}t = \frac{1}{2(\bar{\lambda}^0_{\mathrm{TCTT}} - 1)}\mathrm{d}\delta \tag{4}$$

where $\dot{a}$ is the delamination front speed and dt is a small time increment.

The interlayer in the volume $wh\mathrm{d}a$ will first be delaminated when crossed by the crack fronts and will then undergo the large deformation process in the fast stretching zone. Thus an estimation Π^{th}_{bulk} of the bulk energy density stored and dissipated in the fast stretching zone is given by the work done in a uniaxial tension to stretch the interlayer from 1 to $\bar{\lambda}^*_{\mathrm{TCTT}}$ at a stretch rate $\dot{\lambda} \sim \bar{\lambda}^*_{\mathrm{TCTT}}\dot{a}/h$:

$$\Pi^{th}_{bulk} \approx \int_1^{\bar{\lambda}^*_{\mathrm{TCTT}}-1} \sigma_{\mathrm{T}}\, d\lambda_T \tag{5}$$

with σ_T and λ_T the true stress and stretch values measured during the uniaxial tensile test.

The stretch rates involved in the TCT Test at $h = 0.76$ mm and 10 mm.s^{-1} are about 3 s^{-1}. Using the uniaxial tensile test performed at the same temperature 20 °C and at the closest stretch rate 1 s^{-1} we found $\Pi^T_{bulk} \approx 9$ MJ.m^{-3}. This value is comparable with the one reported in Figure 12.

We remark that this rough estimation should be refined in future work in order to take into account the progressive loss of constraint that the polymer undergoes when being stretched through the regions 2, 3 and 4 in Fig. 13. The purpose of this preliminary modeling is to show that the main component of the macroscopic work of fracture is close to the work of uniaxial extension of the interlayer. Thus, the dissipated portion of this energy can be extracted from the bulk energy density using the dissipation ratio R_d defined previously. In the fast stretching zone, most of the external work is dissipated. In the reference conditions of the TCT Test 85% of the work done on the fast stretching is zone is dissipated by the viscous and plastic deformation of the polymer.

4.4 Velocity and temperature dependence of the interlayer behavior and of the TCT Test

As the main component of the macroscopic work of fracture is related to the stretching of the interlayer, a qualitative relationship between the large strain uniaxial tensile properties of the interlayer and the TCT Test results can be drawn as a function of loading velocity and temperature. However, the near crack tip work of fracture Γ_{crack} could also depend on the delamination velocity $\dot{a}$ and the temperature in an independent way, and this can indirectly affect the bulk term through a modification of the steady state mean stretch $\bar{\lambda}^0_{\mathrm{TCTT}}$.

The variations of the delamination force F^0_{TCTT} with the applied velocity (Figure 7) can be explained by the behavior of the polymer in uniaxial tension. Indeed, it was found that $\bar{\lambda}^0_{\mathrm{TCTT}}$ was almost constant with applied velocity at a given temperature (Figure 8). Therefore the stress needed to stretch the interlayer in uniaxial tension to an identical stretch increases with increasing average

stretch rate. Similarly, as the steady state mean stretch of the interlayer decreases when the temperature increases, and the interlayer is softer, the delamination force decreases.

The simple description of the TCT Test through the uniaxial tensile behavior of the interlayer, does not however explain the increase of $\bar{\lambda}^0_{\text{TCTT}}$ with velocity observed at 20 °C. The macroscopic stretch plateau reached by the interlayer might be controlled by a balance between the velocity dependence of the resistance to crack propagation Γ_{crack} and that of the polymer hardening at large stretch. Such a dynamic balance is frequently observed in the detachment of soft adhesives where increasing the debonding velocity may decrease or increase the average macroscopic deformation at which the fibril detaches.

Finally, the macroscopic work of fracture depends on loading velocity and temperature as can be seen in Figure 14. Variations similar to the ones of the delamination force are observed: G_m increases when the applied velocity increases and when the temperature decreases. A large drop of G_m is observed when the temperature increases above the glass transition to 50 °C. The combination of these variations could be used to explain the different delamination regimes observed in the TCT Test.

The lower limit instability (low velocity and high temperature) could be linked to the requirement of satisfying both the energetic and stress criterion to propagate the delamination fronts. These minimal energy and minimal stress might also depend on velocity and temperature, but at low imposed velocity the macroscopic work of fracture can be too low to propagate the fronts. Moreover, at low stretch rates and high temperatures, the interlayer is softer, which might also prevent the stress to be high enough.

On the contrary, the upper limit of the TCT Test (high velocities and low temperature), could be linked directly to the limited tear resistance of the interlayer as both the stress and the available energy at the front need to be high enough to initiate and propagate the fracture of the interlayer. This would explain the stable, yet not reproducible, delamination observed at high velocity and low temperature.

5 Conclusion

In the impact rupture of laminated glass, the main source of energy dissipation is provided by the coupled stretching and delamination of the polymer interlayer between broken glass shards. This specific mode of polymer-glass delamination presents some analogy with the peeling of a soft layer in the limit case of vanishing peeling angle[35]. Using the through crack tensile test, we have shown that steady state delamination can be obtained only in a limited range of temperature and applied velocity. In this steady state regime, the delamination force and mean interlayer stretch are constant while four individual delamination fronts propagate in a symmetric manner at constant velocity. Because of the large stretch incurred by the polymer interlayer, this velocity is significantly smaller than the imposed velocity. In fact, our DIC measurements demonstrate that, upon delamination, most of the stretching of the polymer interlayer occurs over a length scale of the order of the interlayer thickness. Beyond this distance, stretching increases much more slowly. Based on this observation, we can evaluate the bulk work of stretching (volume density Π_{bulk}) from the uniaxial tensile response of the polymer measured at the relevant temperature and stretch rate. This estimate is consistent with the value obtained experimentally from the linear evolution of the work of fracture with interlayer thickness. Quite significantly, this linear evolution extrapolates to a non-zero work of fracture at zero thickness. This extrapolation signals massive dissipation near the crack tip, with a work of fracture $\Gamma_{crack} = 2$ kJ.m^{-2} smaller yet comparable to the bulk stretch contribution. This value, however, is still thousandfold larger than the energy required to break the interfacial hydrogen bonds[36], because of strong material dissipation around the crack tip. Further work will investigate the connection between these two dissipation processes in an attempt to establish the relation between applied force (or mean stretch) and delamination velocity.

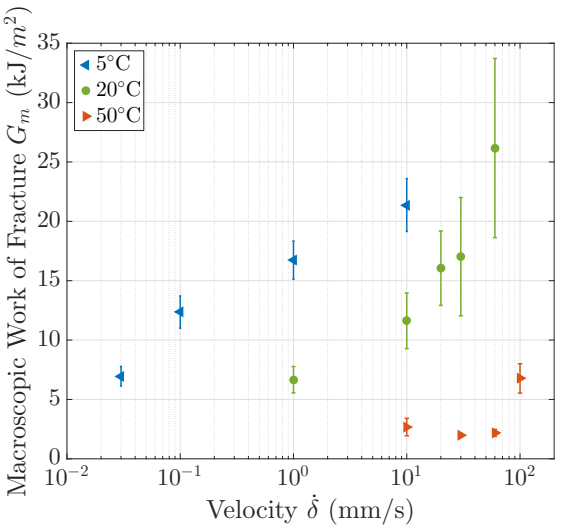

Fig. 14 Variations of the macroscopic work of fracture G_m provided during the TCT Test at h = 0.76 mm for different temperatures (5, 20 and 50 °C) and different velocities.

6 Acknowledgements

We thank A. Jagota, C.Y. Hui and R. Gy for fruitful discussions.

References

1 P. Hooper and B. Blackman, *Journal of Material Science*, 2012, **47**, 3564–3576.

2 F. Flocker and L. Dharani, *Engineering Structures*, 1997, **19**, 851–856.

3 X. Xu, B. H. Liu, Y. Wang, Y. B. Li and J. Xu, *Journal of Physics: Conference Series*, 2013, **451**, 1–7.

4 Y. Sha, C. Y. Hui, E. Kramer, P. Garret and J. Knapczyk, *Journal of adhesion science and technology*, 1997, **11**, 49–63.

5 S. Muralidhar, A. Jagota, S. Bennison and S. Saigal, *Acta Materialia*, 2000, **48**, 4577–4588.

6 C. Butchart and M. Overend, International Conference at glasstec, Düsseldorf, Germany, 2012.

7 P. Rahulkumar, A. Jagota, S. Bennison, S. Saigal and S. Muralidhar, *Acta Materialia*, 1999, **47**, 4161–4169.

8 R. Schapery, *International Journal of Fracture*, 1975, **11**, 141–159.

9 P. de Gennes, *Compte Rendu de l'Académie des Sciences Paris*, 1988, **307**, 1949–1953.

10 A. Gent, *Langmuir*, 1996, **12**, 4492–4496.

11 C. Creton and M. Ciccotti, *Reports on Progress in Physics*, 2016, **79**, 046601.

12 T. Ondarçuhu, *J. Phys. II France*, 1997, **7**, 1893–1916.

13 P. Elziere, *Ph.D. thesis*, Université Pierre et Marie Curie, 2016.

14 F. Hild and S. Roux, *Correli Q4: A Software for Finite-element Displacement Field Measurements by Digital Image Correlation*, ENS Cachan Internal report 269, 2008.

15 E. Nourry, *Ph.D. thesis*, Ecole supérieure d'Arts et Métiers, 2005.

16 A. N. Gent and S.-M. Lai, *Journal of Polymer Science Part B: Polymer Physics*, 1994, **32**, 1543–1555.

17 A. N. Gent, S.-M. Lai, C. Nah and C. Wang, *Rubber Chemistry and Technology*, 1994, **67**, 610–618.

18 F. Saulnier, T. Ondarcuhu, A. Aradian and E. Raphael, *Macromolecules*, 2004, **37**, 1067–1075.

19 B. Persson, O. Albohr, G. Heinrich and H. Ueba, *Journal of Physics: Condensed Matter*, 2005, **17**, R1071–R1142.

20 E. Barthel and C. Fretigny, *Journal of Physics D: Applied Physics*, 2009, **42**, 195302–195311.

21 C.-Y. Hui, A. Jagota, S. J. Bennison and J. D. Londono, *Proceedings of the Royal Soiety of London A*, 2003, **459**, 1489–1516.

22 R. Villey, C. Creton, P. Cortet, M. Dalbe, T. Jet, B. Saintyves, S. Santucci, L. Vanel, D. Yarusso and M. Ciccotti, *Soft Matter*, 2015, **11**, 3480–3491.

23 R. R. Collino, N. R. Philips, M. N. Rossol, R. M. McMeeking and M. R. Begley, *Journal of The Royal Society Interface*, 2014, **11**, 20140453–20140453.

24 S. Ponce, J. Bicot and B. Roman, *Soft Matter*, 2015, **48**, 9281–9290.

25 N. Amouroux, J. Petit and L. Leger, *Langmuir*, 2001, **17**, 6510–6517.

26 B. Newby and M. Chaudhury, *Langmuir*, 1997, **13**, 1805–1809.

27 B. Newby and M. Chaudhury, *Langmuir*, 1998, **14**, 4865–4872.

28 B. Cotterell and J. Reddel, *International Journal of Fracture*, 1977, **13**, 267–277.

29 J. Karger-Kocsis, T. Czigány and E. Moskala, *Polymer*, 1998, **39**, 3939–3944.

30 C. Plummer, P. Scaramuzzino, H.-H. Kausch, R. Steinberger and R. W. Lang, *Polymer Engineering & Science*, 2000, **40**, 985–991.

31 F. Deplace, C. Carelli, S. Mariot, H. Retsos, A. Chateauminois, K. Ouzineb and C. Creton, *The Journal of Adhesion*, 2009, **85**, 18–54.

32 D. Yarusso, *The Journal of Adhesion*, 1999, **70**, 299–320.

33 E. J. Kramer and L. L. Berger, in *Fundamental processes of craze growth and fracture*, Springer Berlin Heidelberg, 2005, pp. 1–68.

34 P. Miller and E. J. Kramer, *Journal of Materials Science*, 1991, **26**, 1459–1466.

35 K. Kendall, *Journal of Physics D: Applied Physics*, 1975, **8**, 1449–1452.

36 J. N. Israelachvili, *Intermolecular and Surface Forces*, Academic Press, New York, 2nd edn., 1992.